Research Article

Journal of Applied Toxicology

Received: 14 July 2014, Revised: 12 August 2014, Accepted: 17 August 2014 Published online in Wiley Online Library: 16 September 2014

(wileyonlinelibrary.com) DOI 10.1002/jat.3073

Hepatotoxicity and liver injury induced by hydroxyapatite nanoparticles

Qingqing Chen, Yang Xue and Jiao Sun*

ABSTRACT: As hydroxyapatite nanoparticles (HA NPs) are increasingly used in biomedical and biotechnological fields, risk assessment of HA NPs has attracted extensive attention. Nevertheless, little is known about the potential adverse effects of HA NPs on normal hepatocytes and the liver. In the present study, we conducted an *in vitro* study in which 80-nm HA NPs were incubated with normal Buffalo rat liver (BRL) cells. By analyzing the changes in cell viability, apoptosis/necrosis and the mitogen-activated protein kinase (MAPK) signaling pathway, we investigated the cytotoxicity and potential mechanism of HA NPs in hepatocytes. Furthermore, we used the serum hematology and histopathology examinations to explore the *in vivo* effects of HA NPs on the structure and function of the liver. Our results showed that exposure to HA NPs at a concentration above 200 $\mu g\,ml^{-1}$ decreased cell viability, increased levels of lactate dehydrogenase (LDH) leakage, induced apoptosis and necrosis, and triggered the MAPK signaling pathway in BRL cells in a dose-dependent manner. Moreover, our *in vivo* study indicated that HA NPs increased the white blood cell count (WBC) and the levels of tumor necrosis factor-α (TNF-α), aspartate aminotransferase (AST) and alanine aminotransferase (ALT) in the serum, caused inflammatory cell infiltration at the portal area in the liver, and induced hepatic oxidative stress with elevated levels of hydrogen peroxide (H_2O_2) and malondialdehyde (MDA). These data demonstrate that at certain concentrations, 80-nm HA NPs cause hepatotoxicity and liver injury. Copyright © 2014 John Wiley & Sons, Ltd.

Keywords: hydroxyapatite nanoparticles; hepatotoxicity; liver; MAPK; oxidative stress

Introduction

Hydroxyapatite nanoparticles (HA NPs), one of the most successful biomaterials, have been widely used as drug carriers (Matsumoto *et al*., 2004; Xu *et al*., 2007) and scaffold materials for bone repair and tissue engineering (Laschke *et al*., 2007; Huber *et al*., 2008). The wide-spread application of HA NPs enhances the probability of human exposure and environmental release and their small size and large surface area provide these nanoparticles with the potential to induce toxicity after they enter the human body. The liver is the major organ for the biotransformation of toxins and is also the primary target organ for exposure to nanoparticles that can enter into the bloodstream (Xie *et al*., 2011, 2012). In our previous study, Sun and Xie (2011) found that HA NPs predominantly accumulate in the liver after administration via intravenous (i.v.) injection and are retained in the liver for over 28 days. Could these HA NPs cause harmful biological responses in the liver? We are very interested in this question and attempt to answer it in the present study. It is also imperative to assess the safety of HA NPs for their use in clinical applications.

Liver tissue is mainly composed of hepatocytes, and recent studies have shown that nanoparticles, such as titanium dioxide nanoparticles and copper oxide nanoparticles, can induce toxicity in hepatocytes (Petkovic *et al*., 2011; Piret *et al*., 2012). Yuan *et al*. (2010) also found that HA NPs inhibit cell viability and lead to apoptosis in human hepatoma HepG2 cells. Moreover, silica nanoparticles, gold nanoparticles and iron oxide nanoparticles were all reported to accumulate primarily in the liver and cause inflammatory responses, necrosis, fibrosis and/or metabolic dysfunction in the liver tissue after they enter into the bloodstream (Nishimori *et al*., 2009; Abdelhalim and Jarrar, 2011; Feng *et al*., 2011; Lu *et al*., 2011). However, few studies have attempted to investigate the hazardous effects of HA NPs on normal hepatic cells and liver tissue; the detailed mechanisms of their toxicity are unknown.

The MAPK pathway, which is composed of three distinct signaling modules, the c-Jun N-terminal kinase (JNK) cascade, the p38 MAPK cascade and the extracellular signal-regulated kinase (ERK) cascade, plays a crucial role in the regulation of many cellular processes, such as cell growth and proliferation, differentiation and apoptosis (Chang and Karin, 2001). Recently, the involvement of the MAPK pathway in the induction of apoptosis by nanoparticles has been demonstrated (Hsin *et al*., 2008; Kang *et al*., 2009; Liu and Sun, 2010; Wu *et al*., 2010). HA NPs have been reported to lead to apoptosis in several types of cells (Sun and Ding, 2009; Wang *et al*., 2012; Xu *et al*., 2012). However, whether the MAPK signaling pathway is involved in the cytotoxicity of HA NPs is unknown.

In the present study, we conducted *in vitro* experiments in which HA NPs were incubated with normal Buffalo rat liver (BRL) cells. By analyzing the changes in cell viability, and the MAPK signaling pathway, we investigated the cytotoxicity and potential mechanism of HA NPs in hepatocytes. Furthermore, we performed serum biochemistry and hematology and histopathology examinations to systematically investigate the liver injury induced by HA NPs *in vivo*.

*Correspondence to: Jiao Sun, No.427, Ju-men Road, Shanghai 200023, China. Email: jiaosun59@yahoo.com

Shanghai Biomaterials Research & Testing Center,Shanghai Key Laboratory of Stomatology, Ninth People's Hospital, Shanghai Jiaotong University School of Medicine, Shanghai 200023, China

Journal of Applied Toxicology

Materials and method

Characterization and dispersion of HA NPs

HA NPs at ≥ 99.0% purity were purchased from Nanjing Emperor Nano Material Company Ltd (Nanjing, China). The diameters of the HA NPs were confirmed by transmission electron microscopy (TEM, JEM-2010; JEOL Ltd., Tokyo, Japan). The size and zeta potential of HA NPs in high-glucose Dulbecco's modified Eagles medium (DMEM; Gibco-Invitrogen Co., Paisley, UK) containing 10% fetal bovine serum (FBS; Gibco-Invitrogen Co.) or physiological saline were determined with a Zetasizer 3000HS system (Malvern Instruments Ltd., Worcestershire, UK) and a laser diffraction particle size analyzer (LS230, Beckman Coulter, Inc., Brea, CA, USA).

First, the HA NPs were sterilized using ethylene oxide. For the *in vitro* studies, the HA NPs were suspended at concentrations of 25, 50, 100, 200, 400 and 800 $\mu g\,ml^{-1}$ in high-glucose DMEM containing 10% FBS, 100 U ml^{-1} penicillin and 100 $\mu g\,ml^{-1}$ streptomycin (Gibco-Invitrogen Co.). For the *in vivo* studies, a HA NP stock solution was prepared at a concentration of 5 $mg\,ml^{-1}$ in physiological saline. To reduce aggregation and produce a uniform suspension, all samples were sonicated for at least 20 min before use.

Cell preparation and culture

The normal BRL cell line was obtained from the Cell Bank of the Type Culture Collection of the Chinese Academy of Sciences (Shanghai, China). The BRL cells were grown in high-glucose DMEM containing 10% (v/v) heat-inactivated FBS and 100 U ml^{-1} penicillin/streptomycin at 37 °C and 5% CO_2. After the cells had been attached to the culture surface for 24 h in this medium, freshly sonicated HA NP suspensions were immediately applied to the cells. Cells that were not exposed to HA NPs were used as a control in each *in vitro* assay.

Cellular uptake of HA NPs

TEM was used to visualize cellular uptake of HA NPs by BRL cells. Briefly, BRL cells were plated in a plastic culture flask at a density of 1×10^6 cells ml^{-1} and allowed to attach for 24 h. Then the cells were treated with HA NPs (800 $\mu g\,ml^{-1}$) for 1 h. After the treatment, the cells were washed with phosphate-buffered saline, prefixed with 2% glutaraldehyde, stained with 1% osmium tetroxide and embedded in Spurr's resin to enable viewing by TEM.

Cell viability assay and lactic dehydrogenase (LDH) measurement

BRL cell viability was determined using a Cell Counting Kit-8 (CCK-8; Beyotime Biotech Ltd., Nantong, China). Briefly, BRL cells were plated in a 96-well plate at a density of 5×10^3 cells per well and allowed to attach for 24 h. Then the BRL cells were treated with culture media containing different concentrations of HA NPs for 24 h. After the treatment, the cells were incubated with CCK-8 for 2 h, and the absorbance at 450 nm was measured using a microplate reader (Wellscan MK3; Labsystems, Dragon, Finland). The survival rate of each dose was calculated from the relative absorbance at 450 nm and expressed as a percentage of the control.

The amount of LDH leakage was determined using a commercial LDH kit (Jiancheng, Nanjing, China), which is based on the measurement of LDH activity in the extracellular medium. After the exposure of the BRL cells to the HA NPs for 24 h, the cell culture medium was collected for LDH measurement according to the manufacturer's protocol, and the absorbance at 440 nm was measured using a UV-visible spectrophotometer (UV-8500; TianMei, Shanghai, China).

Assessment of necrosis and apoptosis

Apoptosis was measured using an Annexin V-FITC/propidium iodide (PI) apoptosis detection kit (BD Biosciences, San Diego, CA, USA). Briefly, BRL cells were exposed to HA NPs for 24 h, washed three times with PBS and trypsinized. After centrifugation at 161 g, the cell pellet was washed once with PBS, incubated with 5 ml of Annexin V-FITC for 10 min, and then stained with 5 ml of PI. The samples were diluted with 200 ml of binding buffer and analyzed with a FAC-Scan flow cytometer (Becton Dickinson, San Jose, CA, USA). A least 1×10^4 cells were counted for each sample. The cell population of interest was gated based on forward and side-scatter. The vertical and horizontal lines were drawn based on the auto fluorescence of the untreated control cells. The different labeling patterns in the Annexin V-PI analysis corresponded to different cell populations in which FITC-negative and PI-negative cells were designated as viable cells, the FITC-positive and PI-negative cells were designated as early apoptotic cells, the FITC-positive and PI-positive cells were designated as late apoptotic cells, and the FITC-negative and PI-positive cells were designated as necrotic cells. Data analysis was performed using Cell Quest software (Becton Dickinson).

Western blot analysis

Total cellular protein extracts were prepared as described in our previous study (Liu and Sun, 2010). Briefly, BRL cells were treated with HA NPs in a 6-well plate for 24 h, washed once with ice-cold PBS and lysed in ice-cold lysis buffer [50 mM Tris-HCl, 150 mM NaCl, 1% NP-40, 0.1% sodium dodecyl sulfate (SDS); Applygen, Beijing, China] containing 1 mM phenylmethylsulphonyl fluoride (PMSF; Sigma, St. Louis, MO, USA) for 30 min. After centrifugation of the lysates at 24149 g and 4 °C for 10 min, the supernatants were collected and stored at 80 °C until use. The protein concentrations of these extracts were determined using the BCA method.

Western blot analysis of p-ERK, ERK, p-p38, p38, p-JNK and JNK was performed using their respective antibodies. Briefly, equal amounts of protein lysate (40–80 μg) were loaded separated on SDS-polyacrylamide gels and electrophoretically transferred to nitrocellulose (NC) membranes (GE Amersham Biosciences, USA). After blocking with 5% non-fat milk in Tris-buffered saline containing 0.05% Tween-20 (TBST) for 1 h at room temperature, the membrane was incubated with antibodies against p-EKR, ERK, p-p38, p38, p-JNK, JNK or β-actin (1:1000, rabbit monoclonal; Cell Signaling Technology, Inc., BSN, USA) overnight at 4 °C, washed with TBST, and incubated with a horseradish peroxidase-conjugated anti-rabbit IgG secondary antibody for 1 h at 37 °C. The antibody-bound proteins were detected by an enhanced chemiluminescence kit (Millipore, Billerica, MA, USA). Bio-Rad Quantity One software (Bio-Rad, Richmond, CA, USA) was used to perform the densitometric scanning.

Animals and treatment

The animal study was approved by the Animal Ethics Committee of Shanghai Jiaotong University (China). A total of 12 male Sprague–Dawley (SD) rats (8 week old and weighing approximately 200 g) were purchased from the Shanghai Laboratory Animal Center of the Chinese Academy of Sciences (SLACCAS; Shanghai, China). One week prior to the beginning of the experiment, the rats were housed in pairs under controlled environmental conditions (temperature 23 ± 0.5 °C, humidity 50 ± 5%, lights on 07:00–19:00 h). The rats were allowed free access to standard rat chow and water. After 1 week of acclimation, six rats were randomly selected as the control group and the remaining six rats were assigned to the HA NP group.

After an overnight fast, HA NPs were administered to the rats in a single dose of 50 mg kg^{-1} by i.v. injection into the tail vein, whereas the controls were injected with vehicle (physiological saline). At 48 h post-injection, blood samples from the rats were collected and used for clinical biochemical analysis and hematological studies. The left lateral lobe of the liver was removed and cut into two pieces immediately after termination. One piece was used for histopathology and the other was snap-frozen in liquid nitrogen and stored at −80 °C until oxidative biomarker analyzes were performed.

Histopathology

All tissue samples were harvested and immediately fixed in a 10% formalin solution. The histopathological tests were performed using standard laboratory procedures. Briefly, the tissues were embedded in paraffin blocks, sectioned into 5-μm slices, and then mounted onto glass slides. After hematoxylin and eosin (H&E) staining, the sections were evaluated and photos were taken using an optical microscope. The analysis of the sections was performed by a blinded to pathologist.

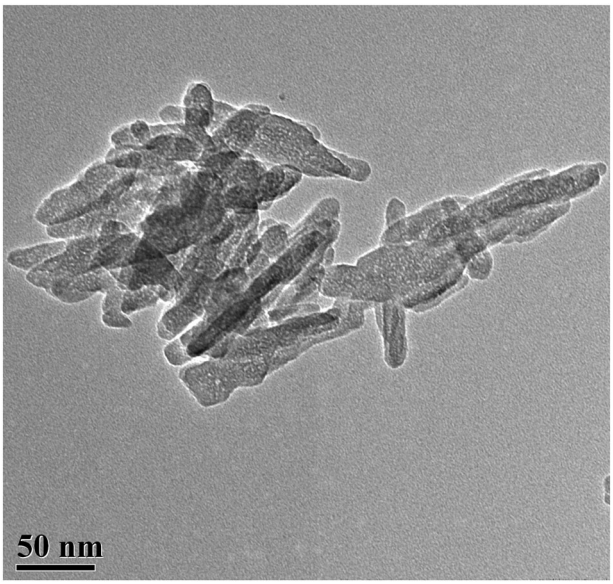

Figure 1. Transmission electron microscopy (TEM) image for hydroxyapatite nanoparticles (HA NPs).

Hematological analysis and clinical chemistry

Hematological parameters, including the white blood cell count (WBC), neutrophils (NEU), lymphocytes (LYM), monocytes (MONO), erythrocytes (RBC), hemoglobin (HGB) and platelet count (PLT), were measured with a hematological autoanalyzer (Coulter T540 hematology system; Beckman Coulter, Inc.).

Clinical chemistry analysis of the serum samples was carried out with a Cobas Integra 400Plus Automatic Biochemistry Analyzer (Roche, Basle, CH-BS). The following parameters were tested: alanine aminotransferase (ALT), aspartate aminotransferase (AST), alkaline phosphatase (ALP), total bile acid (TBA), blood urea nitrogen (BUN), cholesterol (CHOL), triglyceride (TG), uric acid (UA), LDH and low-density lipoprotein (LDL). In addition, the tumor necrosis factor (TNF)-α level in the serum was measured using an ELISA kit (ExCell Bio, Shanghai, China).

Oxidative stress-related biomarker assay

The livers from each group were weighed, and cold protein lysis buffer was added at a ratio of 1:9 (w/v). The mixtures were homogenized at 4 °C using an ultrasonic cell disruptor (Vibra-Cell VCX105; Sonics, Branson, MO, USA). The solution was then centrifuged at 12 000 g and 4 °C for 10 min. The supernatants were collected for oxidative biomarker analysis. The activities of GSH and SOD and the levels of hydrogen peroxide (H_2O_2) and malondialdehyde (MDA) in the liver extracts were examined. All commercial colorimetric assay kits were purchased from Beyotime Biotech Ltd. (Nantong, China) and the assays were performed according to the manufacturer's instructions. Protein concentrations were determined using the BCA method.

Statistical analysis

The data are expressed as the mean ± standard deviation. Statistical analyzes were performed using SPSS software (v 12.0; IBM Corporation, Armonk, NY, USA), and statistical comparisons were analyzed using Student's *t*-test and one-way ANOVA followed by Tukey's honestly significant difference (HSD) post hoc test. Differences were considered statistically significant when $P < 0.05$ or $P < 0.01$.

Table 1. Hydrodynamic diameter and zeta potential of hydroxyapatite nanoparticles (HA NPs)

Particles	Hydrodynamic diameter in DMED medium with 10% FBS	Hydrodynamic diameter in physiological saline	Zeta potential in DMED medium with 10% FBS	Zeta potential in physiological saline
HA NPs	278.2 nm	245.1 nm	-12.4	-16.3

The diameters of the HA NPs were confirmed by transmission electron microscopy (TEM). The size and zeta potential of HA NPs in high-glucose Dulbecco's modified Eagles medium (DMEM) containing 10% fetal bovine serum (FBS) or physiological saline were determined with a Zetasizer 3000HS system and a laser diffraction particle size analyzer.

Journal of Applied Toxicology

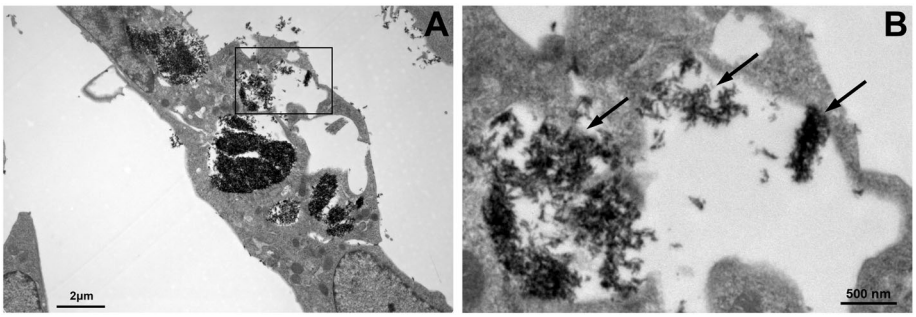

Figure 2. Transmission electron microscopy (TEM) image of cellular uptake hydroxyapatite nanoparticles (HA NPs) by Buffalo rat liver (BRL) cells. BRL cells were treated with HA NPs (800 μg ml^{-1}) 1 h. (A) Image of the whole cell. (B) Image of the gated part of (A). HA NPs are indicated with black arrows.

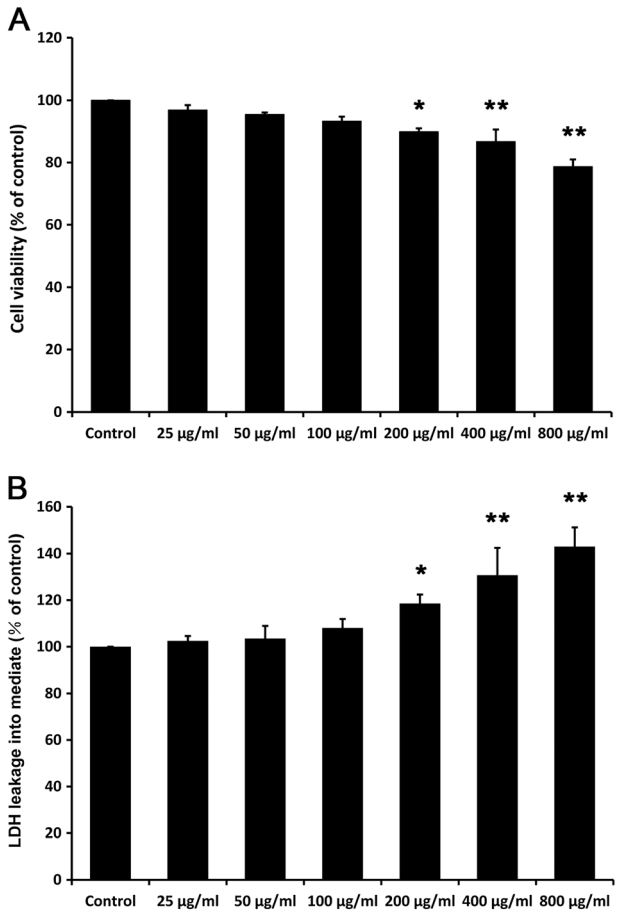

Figure 3. Effects of hydroxyapatite nanoparticles (HA NPs) on the viability and lactic dehydrogenase (LDH) leakage of Buffalo rat liver (BRL) cells. BRL cells were treated with culture media containing different concentrations (25, 50, 100, 200, 400 and 800 μg ml^{-1}) of HA NPs for 24 h. (A) The viability of BRL cells measured by the CCK-8 assay; (B) The LDH leakage in the supernatants of BRL cells measured by the LDH assay. Normal BRL cells that were not exposed to HA NPs were used as control. Data represent mean ± SD, $n = 3$, $^{*}P < 0.05$ when compared with the control, $^{**}P < 0.01$ when compared with the control.

Results

Characterization of HA NPs

As shown in the TEM image in Fig. 1, the HA NPs employed in this study were needle like with a long diameter of 80 nm and a short diameter of 20 nm. The sizes of HA NPs and their agglomerates when suspended in either DMEM containing 10% FBS or physiological saline were estimated using dynamic light scattering (DLS). The results (Table 1) showed that the agglomeration of the HA NPs was 278.2 nm in cell culture medium and 245.1 nm in physiological saline, larger than the particle size measured by TEM. The zeta potential values were −12.4 and −16.3 mV in cell culture medium and physiological saline, respectively (Table 1).

Cellular uptake of HA NPs by BRL cells

The cellular uptake of HA NPs by BRL cells after exposure to HA NPs (800 μg ml^{-1}) for 1 h was examined by TEM. As shown in Fig. 2A, small particle aggregates were visible. Some small particle aggregates were localized in the cytoplasmic vesicles of the cell, whereas some aggregates were free in the cytoplasm (Fig. 2B).

Effects of HA NPs on cellular viability and LDH leakage of BRL cells

Cell proliferation in response to different concentrations of HA NPs was evaluated by the CCK8 assay. As shown in Fig. 3A, at lower treatment concentrations (25–100 μg ml–1), the HA NPs did not affect the viability of the BRL cells. However, at treatment concentrations of 200 μg ml^{-1} and higher, the HA NPs induced concentration-related decreases in the survival of the BRL cells ($P < 0.05$ or 0.01).

The cytotoxicity of the HA NPs was also evaluated by the levels of LDH in the culture medium of the BRL cells. As shown in Fig. 3B, the HA NPs induced apparent LDH leakage from BRL cells treated for 24 h at a concentration range of 200–800 μg ml^{-1} ($P < 0.05$ or 0.01), revealing the impact of these nanoparticles on cell membrane integrity.

Effects of HA NPs on apoptosis and necrosis in BRL cells

To investigate the extent of damage induced by the HA NPs, apoptosis and necrosis in the BRL cells were assessed by staining with Annexin V-FITC and PI followed by flow cytometry. As shown in Fig. 4, when the BRL cells were treated with HA NPs at concentrations of 400 and 800 μg ml^{-1} for 24 h, the number of apoptotic and necrotic cells increased in a dose-dependent manner ($P < 0.05$ or 0.01).

Effects of HA NPs on the MAPK signaling pathway in BRL cells

To further understand the signal transduction pathways involved in HA NP-induced cell death, BRL cells were exposed to HA NPs for the

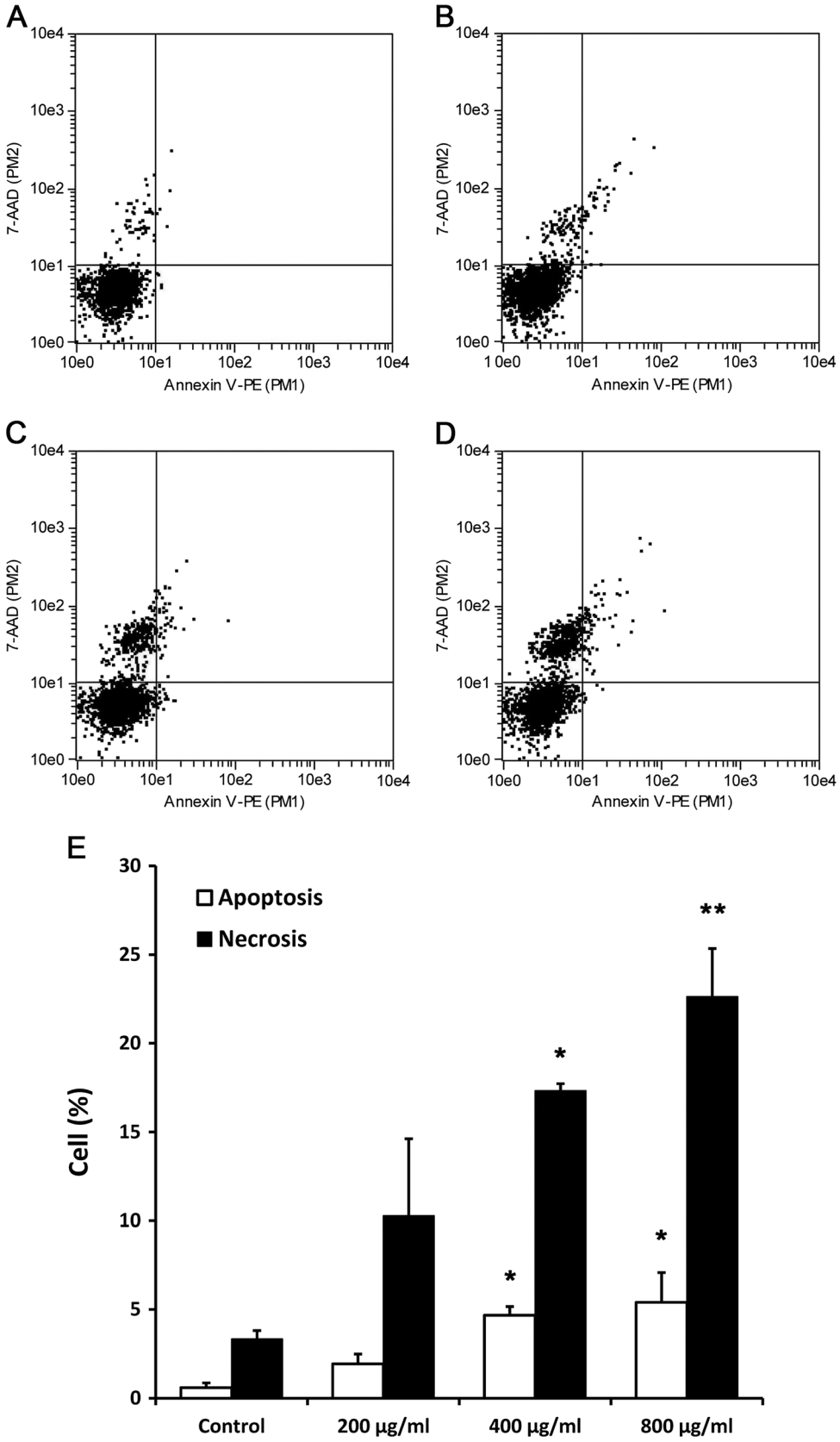

Figure 4. Effects of hydroxyapatite nanoparticles (HA NPs) on apoptosis and necrosis in Buffalo rat liver (BRL) cells. After BRL cells were treated with increasing concentrations of HA NPs for 24 h, Annexin V-FITC/PI double staining was used to analysis the cell apoptosis and necrosis. (A) Control; (B) HA NPs 200 μg ml^{-1}; (C) HA NPs 400 μg ml^{-1}; (D) HA NPs 800 μg ml^{-1}; (E) Percentages of apoptosis and necrosis in BRL cells. Normal BRL cells that were not exposed to HA NPs were used as a control. Data represent mean ± SD, $n = 3$, *$P < 0.05$ when compared with the control, **$P < 0.01$ when compared with the control.

Journal of Applied Toxicology

analysis of p-ERK, ERK, p-p38, p38, p-JNK and JNK by Western blot. As shown in Fig. 5, the phosphorylation of p38 was increased in a dose-response manner in the BRL cells exposed to 200 to 800 μg ml^{-1} HA NPs for 24 h ($P < 0.05$ or 0.01), the phosphorylation of ERK and JNK were increased in a dose-response manner at concentrations of 400 and 800 μg ml^{-1} HA NPs ($P < 0.05$ or 0.01), whereas the expression of total p38, ERK and JNK did not change ($P > 0.05$).

Histopathology examination

Morphological alterations of the liver tissues were observed by hematoxylin and eosin (H&E) staining. As shown in Fig. 6A, the control liver tissues had normal histology. However, the liver tissues from the rats exposed to the HA NPs showed inflammatory cell infiltration at the portal area in the liver (Fig. 6B).

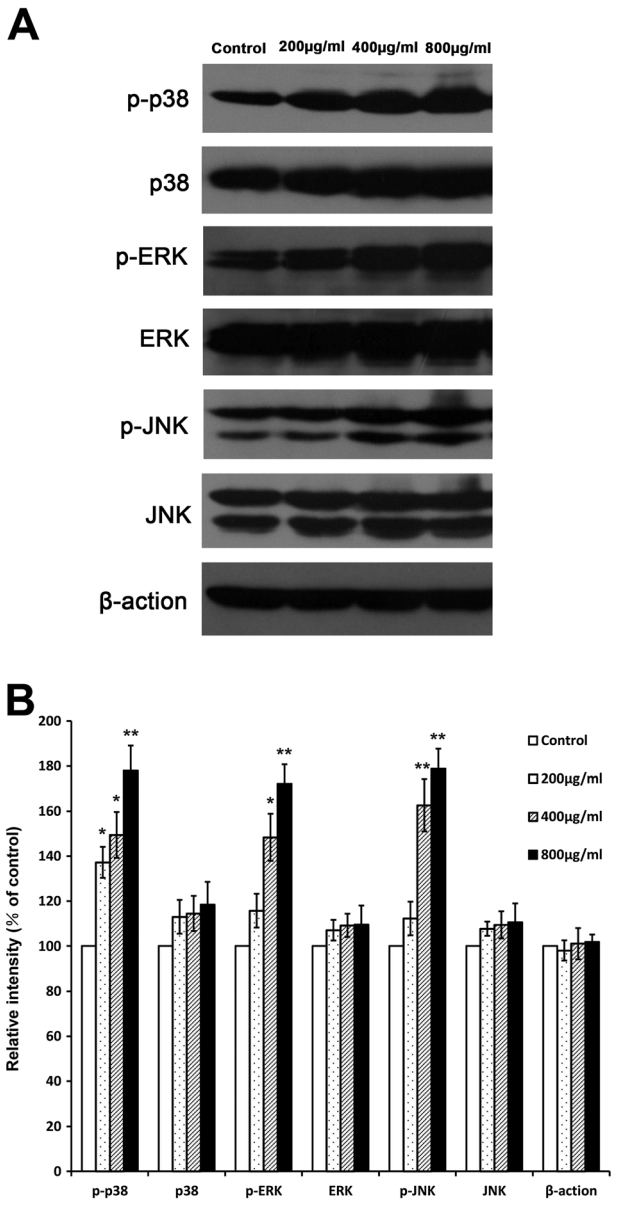

Figure 5. Effects of hydroxyapatite nanoparticles (HA NPs) on the MAPK signaling pathway in Buffalo rat liver (BRL) cells. (A) After BRL cells were treated with increasing concentrations of HA NPs for 24 h, the protein of p-EKR, ERK, p-p38, p38, p-JNK and JNK expression was detected via western blot analysis. β-Actin was used as an internal control to monitor for equal loading. Normal BRL cells that were not exposed to HA NPs were used as control. (B) Densitometry showing data from three experiments. Data represent mean ± SD, $n = 3$, $^{*}P < 0.05$ when compared with the control, $^{**}P < 0.01$ when compared with the control.

Hematological analysis and clinical chemistry

The hematological analysis showed that the WBC was increased in the HA NP group (Table 2). The serum level of the inflammatory cytokine TNF-α was also elevated in the HA NP group. In addition, significant changes in the clinical biochemistry parameters of the serum were observed after the administration of HA NPs to rats (Table 3). The ALT, AST, TBA, CHOL, UA, LDH and LDL in the HA NP group were all increased compared with the control group ($P < 0.05$).

Oxidative damage in the liver

The changes in the levels of H_2O_2, GSH, SOD and MDA in the liver after HA NP administration are presented in Fig. 6. Compared to the control, the livers of rats treated with the HA NPs exhibited an increase in the levels of H_2O_2 and MDA and a decrease in the level of GSH ($P < 0.05$).

Discussion

HA NPs have been widely used as reconstructive and prosthetic materials for the repair and regeneration of osseous tissue (Laschke *et al*., 2007; Huber *et al*., 2008). They also have potential applications in drug delivery (Matsumoto *et al*., 2004; Xu *et al*., 2007). While the beneficial aspects of HA NPs are widely publicized, whether they act like other nanoparticles, such as silica nanoparticles, whose small size and high surface activity have the potential to induce toxicity (Ye *et al*., 2010), is unknown. This is the question we concern and attempt to answer. Because HA NPs accumulate primarily in the liver after they enter into the bloodstream (Sun and Xie, 2011), understanding whether HA NPs exert adverse effects on normal hepatocytes and how these nanoparticles interact with liver tissue is essential.

In this study, normal rat hepatic (BRL) cells were selected to investigate the hepatotoxicity induced by HA NPs *in vitro*. Under TEM, we observed that HA NPs were readily taken up by BRL cells (Fig. 2). Some small HA NP aggregates were localized in the cytoplasmic vesicles of the cell, which might indicate their uptake via incorporation of particles into the membrane, e.g. endocytosis. However, some HA NP aggregates were free in the cytoplasm, which might cause damage to the subcellular structure near the particles (Xue *et al*., 2014). Our study showed that the cellular uptake of HA NPs induce a dose-dependent cytotoxicity in the BRL cells, as detected by the expression of mitochondrial enzymes by the CCK-8 assay (Fig. 3A). LDH leakage also increased after exposure to the higher concentrations (200–800 μg ml^{-1}) of HA NPs (Fig. 3B). It is well known that LDH is a relatively stable enzyme in cells and can leak out only when the cell membrane is broken (Hussain and Frazier, 2002). Thus, the increase in LDH leakage indicates that exposure to high concentrations of HA NPs can affect cell-membrane integrity and cause damage to BRL cells. To confirm and analyze the hepatotoxicity induced by HA NPs, apoptosis/necrosis was also measured in the present study. The results revealed that BRL cells underwent necrosis and apoptosis at high concentrations (400 and 800 μg ml^{-1}) of HA NPs in a dose-dependent manner (Fig. 4). Necrosis is thought to be unprogrammed cell death that

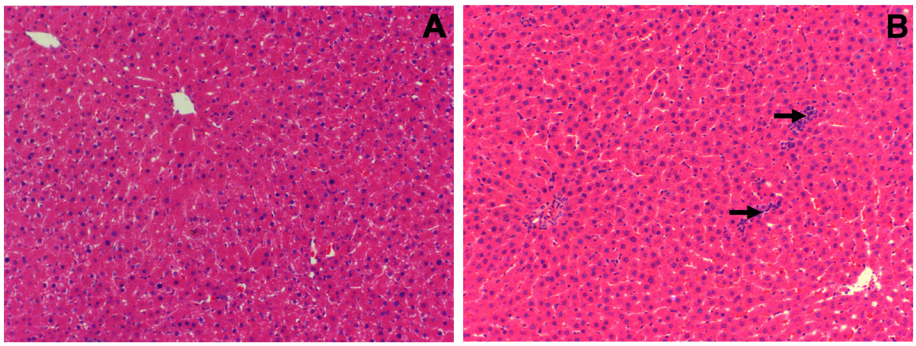

Figure 6. Histological examination. Hydroxyapatite nanoparticles (HA NPs) were administered to the rats in a single dose of 50 mg kg^{-1} by intravenous injection into the tail vein. The SD rats that were injected with physiological saline were used as control. At 48 h post-injection, liver tissues were removed and the liver sections were used for histopathology by hematoxylin–eosin staining. (A) control; (B) HA NP-treated group. Inflammatory cell infiltrates are indicated with black arrows.

Table 2. Effect of hydroxyapatite nanoparticles (HA NPs) on selected clinical hematology parameters

Parameters	Control	HA NPs
WBC (10^9 l^{-1})	4.47 ± 0.63	5.4 ± 0.65 *
LYM (10^9 l^{-1})	3.18 ± 0.56	3.9 ± 0.39
MONO (10^9 l^{-1})	0.07 ± 0.05	0.1
NEU (10^9 l^{-1})	1.27 ± 0.35	1.4 ± 0.41
RBC (10^9 l^{-1})	5.77 ± 0.17	5.88 ± 0.27
HGB (g l^{-1})	118.5 ± 5.63	122 ± 4.52
PLT (10^9 l^{-1})	481.67 ± 47.4	434.2 ± 84.71

HA NPs were administered to the rats in a single dose of 50 mg kg^{-1} by intravenous injection into the tail vein, whereas the controls were injected with physiological saline. At 48 h post-injection, blood samples from the rats were collected and used for hematological studies. WBC: white blood cell count; LYM: lymphocytes; MONO: monocytes; NEU: neutrophils; RBC: erythrocytes; HGB: hemoglobin; PLT: platelet count. Data were presented as mean ± SD, $n = 6$,
* $P < 0.05$ when compared with the vehicle control group.

Table 3. Effect of hydroxyapatite nanoparticles (HA NPs) on selected clinical chemistry parameters

Parameters	Control	HA NPs
ALT (U l^{-1})	81 ± 8.22	97.83 ± 6.94 *
AST (U l^{-1})	150.83 ± 14.19	178.17 ± 19 *
ALP (U l^{-1})	264.16 ± 30.92	289 ± 66.8
TBA (μM)	21.1 ± 4.55	32.5 ± 11.71 *
BUN (mM)	5.78 ± 0.35	5.98 ± 0.5
CHOL (mM)	1.87 ± 0.07	2 ± 0.12 *
TG (mM)	0.6 ± 0.2	0.75 ± 0.27
UA (μM)	68.5 ± 5.4	88.5 ± 11.7 *
LDH (U l^{-1})	1175 ± 158.34	1380.8 ± 188.7 *
LDL (mM)	0.31 ± 0.015	0.385 ± 0.056 *
TNF-α (pg ml^{-1})	44.89 ± 6.49	55.54 ± 9.23 *

HA NPs were administered to the rats in a single dose of 50 mg kg^{-1} by intravenous injection into the tail vein, whereas the controls were injected with physiological saline. At 48 h post-injection, blood samples from the rats were collected and used for clinical biochemical analysis. ALT: alanine aminotransferase; AST: aspartate aminotransferase; ALP: alkaline phosphatase; TBA: total bili acid; BUN: blood urea nitrogen; CHOL: cholesterol; TG: triglyceride; UA: uric acid; LDH: lactic dehydrogenase; LDL: low density lipoprotein; TNF-α: tumor necrosis factor-α. Data were presented as mean ± SD, $n = 6$,
* $P < 0.05$ when compared with the vehicle control group.

is induced by external factors with acute plasma membrane dissolution; thus LDH leakage is most commonly associated with necrotic cell death (Zong and Thompson, 2006). Apoptosis is the process of programmed cell death, which follows a controlled, predictable routine. HA NPs have been reported to induce apoptosis in different types of cells (Sun and Ding, 2009; Wang *et al.*, 2012; Xu *et al.*, 2012).

Therefore, HA NPs induce cytotoxicity in normal hepatocytes, but what is the mechanism? The MAPK family represents a group of proteins involved in the signal transduction of a variety of cellular stimuli and plays a crucial role in the regulation of many cellular processes, such as cell growth and proliferation, differentiation and apoptosis (Chang and Karin, 2001; Hsin *et al.*, 2008). The MAPK pathway is composed of three distinct signaling modules, the ERK, JNK and p38 MAPK cascades. ERK plays a critical role in cell proliferation, differentiation and survival (Czaja *et al.*, 2003). In contrast, JNK and p38 kinase are activated by various toxicants and lead to cell death (Kang *et al.*, 2009; Liu and Sun, 2010; Wu *et al.*, 2010) Our research revealed that HA NPs activated the MAPK signaling pathway, including the JNK, p38 kinase and ERK cascades, by promoting phosphorylation (Fig. 5). The phosphorylation of ERK has been reported to confer resistance to death in hepatocytes (Rosseland *et al.*, 2005; Conde de la Rosa *et al.*, 2006), but in the present study, HA NPs also activated pro-apoptotic pathways, e.g. JNK and p38, which overruled the protective ERK pathway and ultimately led to apoptosis in the BRL cells. Consistent with our results, Cheng *et al.* (2013) also demonstrated that cerium oxide (CeO_2) nanoparticles induce apoptosis in human hepatoma SMMC-7721 cells via the activation of the MAPK signaling pathway.

Because HA NPs can cause damage to normal hepatocytes, will they induce a toxic reaction to liver tissue *in vivo*? Our previous study found that HA NPs were located predominantly in the liver after administration via i.v. injection (Sun and Xie, 2011). In the present study, hematological and histopathological examinations were utilized to determine the effects of HA NPs on liver structure and function. The WBC and TNF-α level were found to be increased in the serum of HA NP-treated rats (Tables 2 and 3).

Journal of Applied Toxicology

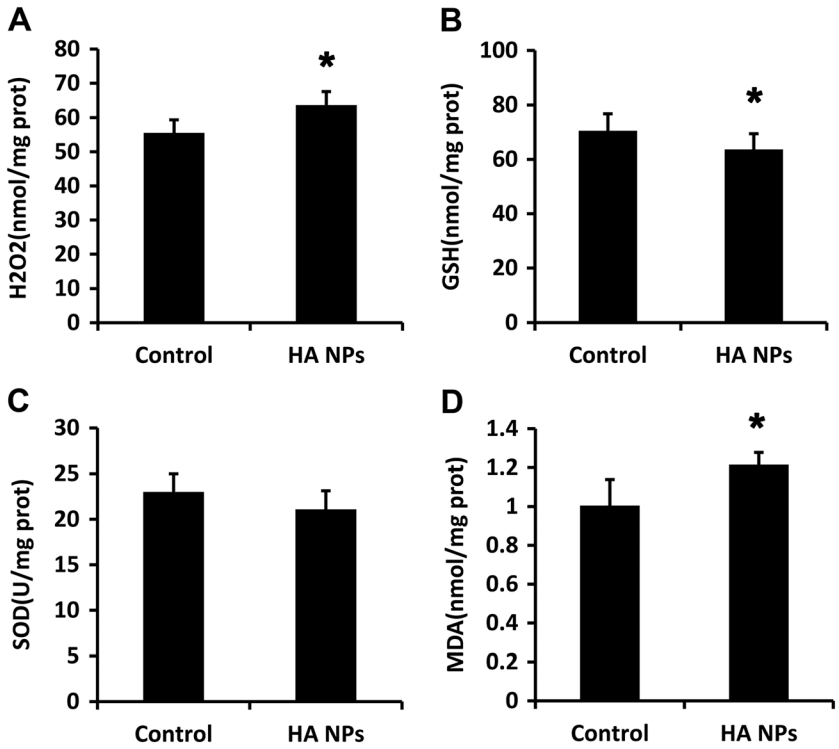

Figure 7. Changes in hydrogen peroxide (H_2O_2), GSH, SOD and malondialdehyde (MDA) levels of the liver tissues. Hydroxyapatite nanoparticles (HA NPs) were administered to the rats in a single dose of 50 mg kg^{-1} by intravenous injection into the tail vein. The Sprague–Dawley (SD) rats that were injected with physiological saline were used as controls. At 48 h post-injection, liver tissues were removed and homogenized for oxidative stress-related biomarker assay. (A) levels of H_2O_2; (B) levels of GSH; (C) levels of SOD; (D) levels of MDA. Data represent mean ± SD, $n = 6$, $^*P < 0.05$ when compared with the control.

Additionally, the liver tissues from the rats exposed to the HA NPs showed inflammatory cell infiltration at the portal area (Fig. 6B). Although HA NPs were reported to have excellent biocompatibility (Matsumoto *et al*., 2004; Laschke *et al*., 2007; Xu *et al*., 2007; Huber *et al*., 2008), as foreign invaders, they can be recognized by the immune system and induce inflammation after they enter the body. ALT and AST are two membrane-bound enzymes that are related to hepatic dysfunction. These enzymes enter into the bloodstream only when the liver is damaged and the hepatic cell membrane is disrupted. Thus, the elevation in the ALT and AST levels in the serum of the HA NP-treated rats indicated liver injury induced by HA NPs.

Furthermore, we examined the oxidative stress levels in the liver tissue. It is well known that oxidative stress can cause oxidative damage to major cellular structures (mitochondria and cytomembrane), macromolecules (DNA, lipids and proteins), leading to cell and tissue damage (Liu and Sun, 2010; Wu *et al*., 2010; Sharma *et al*., 2012). In our study, we observed that exposure to HA NPs caused oxidative stress in the liver, with an elevation of the H_2O_2 and MDA levels and a decrease in the GSH level (Fig. 7). Therefore, we deduced that the observed liver injury might be associated with oxidative stress that was induced by HA NP exposure.

In summary, the present study reveals the potential hepatotoxicity of HA NPs and demonstrates their possible molecular mechanism. Our *in vitro* experiments showed that 80-nm HA NPs are located in BRL cells and at a concentration above 200 μg ml^{-1}, HA NPs decrease cell viability, increase LDH leakage and induce apoptosis and necrosis in BRL cells in a dose-dependent manner. The activation of the MAPK pathway is involved in the mechanism of HA NP-induced hepatocyte injury. Moreover, our *in vivo* experiments demonstrated that HA NPs damage the structure and function of the liver, which may partly be attributed to oxidative stress induced by HA NPs. These data indicate that at certain concentrations, HA NPs have the potential to induce hepatocyte injury and liver damage.

Acknowledgments

This work was supported by grants from the National Natural Science Foundation of China (no 31070843/81271700) and Shanghai Sci-Tech Committee Foundation (no 13DZ2291100).

Conflict of interest

The authors did not report any conflict of interest.

References

Abdelhalim MA, Jarrar BM. 2011. Gold nanoparticles administration induced prominent inflammatory, central vein intima disruption, fatty change and Kupffer cells hyperplasia. *Lipids Health Dis.* **10**:133.

Chang L, Karin M. 2001. Mammalian MAP kinase signaling cascades. *Nature* **410**:37–40.

Cheng G, Guo W, Han L, Chen E, Kong L, Wang L, Ai W, Song N, Li H, Chen H. 2013. Cerium oxide nanoparticles induce cytotoxicity in human hepatoma SMMC-7721 cells via oxidative stress and the activation of MAPK signaling pathways. *Toxicol in Vitro* **27**:1082–1088.

Conde de la Rosa L, Schoemaker MH, Vrenken TE, Buist-Homan M, Havinga R, Jansen PL, Moshage H. 2006. Superoxide anions and hydrogen peroxide induce hepatocyte death by different mechanisms: involvement of JNK and ERK MAP kinases. *J. Hepatol.* **44**:918–929.

Czaja MJ, Liu H, Wang Y. 2003. Oxidant-induced hepatocyte injury from menadione is regulated by ERK and AP-1 signaling. *Hepatology* **37**:1405–1413.

Feng J, Liu H, Bhakoo K, Lu L, Chen Z. 2010. A metabonomic analysis of organ specific response to USPIO administration. *Biomaterials* **32**(27):6558–6569.

Hsin YH, Chen CF, Huang S, Shih TS, Lai PS, Chueh PJ. 2008. The apoptotic effect of nanosilver is mediated by a ROS- and JNK-dependent mechanism involving the mitochondrial pathway in NIH3T3 cells. *Toxicol. Lett.* **179**:130–139.

Huber FX, Berger I, McArthur N, Huber C, Kock HP, Hillmeier J, Meeder PJ. 2008. Evaluation of a novel nanocrystalline hydroxyapatite paste and a solid hydroxyapatite ceramic for the treatment of critical size bone defects (CSD) in rabbits. *J. Mater. Sci. Mater. Med.* **19**:33.

Hussain SM, Frazier JM. 2002. Cellular toxicity of hydrazine in primary hepatocytes. *Toxicol. Sci.* **69**:424–432.

Kang SJ, Kim BM, Lee YJ, Hong SH, Chung HW. 2009. Titanium dioxide nanoparticles induce apoptosis through the JNK/p38-caspase-8-Bid pathway in phytohemagglutinin-stimulated human lymphocytes. *Biochem. Biophys. Res. Commun.* **386**:682–687.

Laschke MW, Witt K, Pohlemann T, Menger MD. 2007. Injectable nanocrystalline hydroxyapatite paste for bone substitution: in vivo analysis of biocompatibility and vascularization. *J. Biomed. Mater. Res. B Appl. Biomater.* **82**:494–505.

Liu X, Sun J. 2010. Endothelial cells dysfunction induced by silica nanoparticles through oxidative stress via JNK/P53 and NF-kB pathways. *Biomaterials* **31**:8198–8209.

Lu X, Tian Y, Zhao Q, Jin T, Xiao S, Fan X. 2011. Integrated metabonomics analysis of the size-response relationship of silica nanoparticles-induced toxicity in mice. *Nanotechnology* **22**:055101.

Matsumoto T, Okazaki M, Inoue M, Yamaguchi S, Kusunose T, Toyonaga T, Hamada Y, Takahashi J. 2004. Hydroxyapatite particles as a controlled release carrier of protein. *Biomaterials* **17**:3807–3812.

Nishimori H, Kondoh M, Isoda K, Tsunoda S, Tsutsumi Y, Yagi K. 2009. Silica nanoparticles as hepatotoxicants. *Eur. J. Pharm. Biopharm.* **72**:496–501.

Petkovic J, Zegura B, Stevanovic M, Drnovsek N, Uskokovic D, Novak S, Filipic M. 2011. DNA damage and alterations in expression of DNA damage responsive genes induced by TiO2 nanoparticles in human hepatoma HepG2 cells. *Nanotoxicology* **5**:341–353.

Piret JP, Jacques D, Audinot JN, Mejia J, Boilan E, Noel F, Fransolet M, Demazy C, Lucas S, Saout C, Toussaint O. 2012. Copper(II) oxide nanoparticles penetrate into HepG2 cells, exert cytotoxicityvia oxidative stress and induce pro-inflammatory response. *Nanoscale* **4**:7168–7184.

Rosseland CM, Wierød L, Oksvold MP, Werner H, Ostvold AC, Thoresen GH, Paulsen RE, Huitfeldt HS, Skarpen E, 2005. Cytoplasmic retention of peroxide-activated ERK provides survival in primary cultures of rat hepatocytes.⊠*Hepatology* **42**:200–207.

Sharma V, Anderson D, Dhawan A. 2012. Zinc oxide nanoparticles induce oxidative DNA damage and ROS-triggered mitochondria mediated apoptosis in human liver cells (HepG2). *Apoptosis* **17**:852–870.

Sun J, Ding T. 2009. p53 Reaction to apoptosis induced by hydroxyapatite nanoparticles in rat macrophages. *J. Biomed. Mater. Res. A* **88A**:673–679.

Sun J, Xie G. 2011. Tissue distribution of intravenously administrated hydroxyapatite nanoparticles labeled with 125I. *J. Nanosci. Nanotechnology* **11**:10996–1000.

Wang L, Zhou G, Liu H, Niu X, Han J, Zheng L, Fan Y. 2012. Nano-hydroxyapatite particles induce apoptosis on MC3T3-E1 cells andtissue cells in SD rats. *Nanoscale* **4**:2894–2899.

Wu J, Sun J, Xue Y. 2010. Involvement of JNK and P53 activation in G2/M cell cycle arrest and apoptosis induced by titanium dioxide nanoparticles in neuron cells. *Toxicol. Lett.* **199**:269–276.

Xie G, Sun J, Zhong G. 2012. Tissular localization and excretion of intravenously administered silica nanoparticles of different sizes. *J. Nanopart. Res.* **14**:671.

Xie G, Wan C, Sun J, Zhong G. 2011. Tissue distribution and excretion of intravenously administered titanium dioxide nanoparticles. *Toxicol. Lett.* **205**:55–61.

Xu Q, Tanaka Y, Czernuszka JT. 2007. Encapsulation and release of a hydrophobic drug from hydroxyapatite coated liposomes. *Biomaterials* **28**:2687–2694.

Xu Z, Liu C, Wei J, Sun J. 2012. Effects of four types of hydroxyapatite nanoparticles with different nanocrystal morphologies and sizes on apoptosis in rat osteoblasts. *J. Appl. Toxicol.* **32**:429–435.

Xue Y, Chen Q, Sun J. 2014. SiO2 nanoparticle-induced impairment of mitochondrial energy metabolism in hepatocytes directly and through a Kupffer cell-mediated pathway in vitro. *Int. J. Nanomed.* **9**:2891–2903.

Ye Y, Liu J, Xu J, Sun L, Chen M, Lan M. 2010. Nano-SiO2 induces apoptosis via activation of p53 and Bax mediated by oxidative stress in human hepatic cell line. *Toxicol. In Vitro* **24**:751–758.

Yuan Y, Liu C, Qian J, Wang J, Zhang Y. 2010. Size-mediated cytotoxicity and apoptosis of hydroxyapatite nanoparticles in human hepatoma HepG2 cells. *Biomaterials* **31**:730–740.

Zong WX, Thompson CB. 2006. Necrotic death as a cell fate. *Genes Dev.* **20**(1):1–15.